Generation of quasimonoenergetic positron beams in chirped laser fields

Suo Tang *

Department of Physics, College of Information Science and Engineering, Ocean University of China, Qingdao, Shandong 266100, China

(Received 23 May 2021; accepted 3 August 2021; published 18 August 2021)

High-energy photons can decay to electron-positron pairs via the nonlinear Breit-Wheeler process when colliding with an intense laser pulse. The energy spectrum of the produced particles is broadened because of the variation of their effective mass in the course of the laser pulse. Applying a suitable chirp to the laser pulse can narrow the energy distribution of the generated electrons and positrons. We present a scenario where a high-energy electron beam is collided with a chirped laser pulse to generate a beam of quasimonoenergetic γ photons, which then decay in a second chirped, UV pulse to produce a quasimonoenergetic source of high-energy electrons and positrons.

DOI: 10.1103/PhysRevA.104.022209

I. INTRODUCTION

When a beam of charged particles collides with an intense laser pulse, the spectrum of produced photons, via the process referred to as the nonlinear Compton scattering (NLC) [1,2], is sensitive to the shape of the pulse. Employing a many-cycle laser pulse will lead to outgoing photon spectra similar to those in a monochromatic background [3,4]: well-defined harmonic fringes in lightfront momenta and emission angle. Collision with short laser pulses will lead to a broadening of outgoing particle harmonic peaks [5–7] and richer spectral structures: infrared structure [8,9], asymmetry in emission angle [10], and pronounced interference phenomena [11,12]. The spectral broadening can be attributed to the inhomogeneous effective mass of the charged particle moving in the intense laser pulse [13–16]: the variation of the effective mass modifies the velocity of the changed particle during the scattering [17–20]. It is also known, that if one can prescribe the chirp of the laser pulse, that is, a nonlinear dependency on the phase, then this relativistic broadening of particle spectra can be compensated for, to generate a narrowband source of high-energy photons [20–22].

The decay of a probe photon to an electron-positron pair in an intense electromagnetic field, is often referred to as the nonlinear Breit-Wheeler process (NBW) [3,23,24], and has been measured experimentally in the landmark E144 experiment more than two decades ago [25,26]. The phenomenology of the process has been investigated theoretically in various types of laser field. First in monochromatic [3] and constant crossed fields [3,27], and more recently in finite laser pulses [28–30], as well as two-color [31] and double-pulse fields [32–34]. As in the NLC process, harmonic structure also arises in the outgoing electron-positron pair spectra operating in a many-cycle laser pulse. However, this structure is only clearly discernible when the center-of-mass energy reaches the threshold of $2mc^2$ already with only a low number of laser photons, where m is electron (positron) rest mass and c is the speed of light.

Analogous to the spectral broadening in the NLC process, the variation of the electron-positron pair's effective mass in the course of the intense laser pulse also induces a broadening in their energy spectra. The current paper is a proof of principle calculation to show that a suitable nonlinear chirp of a laser pulse can also be employed to counterbalance the spectral broadening in the NBW process, and proposes a simple two-step scenario to provide a quasimonoenergetic source positron. The existence of a quasimonoenergetic positron source would be useful in the electron-positron colliding experiments [35–37].

The study of laser chirp's effect on positron spectra is partly motivated by upcoming high-energy experiments LUXE at DESY [38,39] and E320 at FACET-II [40,41], where photons with energies of the order of 10 GeV are planned to be generated, either directly in the laser pulse through Compton scattering of the electrons (LUXE and E320), or from a separated bremsstrahlung and inverse Compton source (LUXE). The multiphoton harmonic regime of the NBW process can be approached by colliding these high-energy photons with the higher-order harmonics of the interaction laser, using, e.g., relativistic plasmas [42–44]. The positron spectra in this regime would show distinct harmonic edges related to multiphoton channels. Colliding with fundamental-frequency [$\omega_0 \sim \mathcal{O}(1\ \mathrm{eV})$] laser pulses, this multiphoton regime apparently cannot be reached as the energy to stimulate the pair production must be provided larger than $2mc^2$ in the center-of-mass frame, and the spectral harmonic edges would be smoothed out as the many-photon channels would be dominant.

The paper is organized as follows. In Sec. II, we present the spectrum of produced positrons in the NBW process, and investigate the contributions from the stationary phase points. We then analyze the broadening of the positron spectrum and propose a special laser frequency chirp to counteract the spectral broadening. In Sec. III we demonstrate numerical implementations of our chirp prescription in narrowing the

*tangsuo@ouc.edu.cn

positron spectra from a single high-energy photon and from the γ ray obtained through the NLC process of a high-energy electron. We conclude in Sec. IV.

II. THEORETICAL FRAMEWORK

We consider the scenario in which a high-energy photon with momentum ℓ colliding (almost) head-on with a laser pulse produces a pair of electron and positron. The laser pulse is simplified as a plane wave with scaled vector potential $a^\mu = |e|A^\mu(\phi)$ and wave vector $k^\mu = \omega_0(1, 0, 0, 1)$ where $\phi = k \cdot x$ and ω_0 is the laser frequency at the initial phase point ϕ_i at which the laser is turned on. The interaction energy is characterized by $\eta_\ell = k \cdot \ell/m^2$. We use natural units $\hbar = c = 1$ throughout and the fine-structure constant is $\alpha = e^2 \approx 1/137$.

The angular-resolved spectrum of the produced positron can be formulated as

$$\frac{d^3P}{ds\, d^2q_\perp} = \alpha \frac{|I|^2 + (SI^* + IS^* - 2FF^*)g(s,1)}{(2\pi)^2 \eta_\ell^2 (1-s)s}, \tag{1}$$

where $g(u, v) = [u^2 + (v - u)^2]/[4u(v - u)]$. We sum over the spin of the outgoing particles and average over the polarization of the incoming photon. The spectrum (1) is parametrized by the three components of the positron momentum p: these are $s = k \cdot p/k \cdot \ell$, the fraction of the photon lightfront momentum taken by the positron, and $q_\perp = (q_x, q_y)$, $q_{x,y} = p_{x,y}/m - s\ell_{x,y}/m$, positron momenta in the plane perpendicular to the laser propagating direction. $q_\perp$ reflects the angular spread of the produced positron around the photon incident direction. In our parameter region, the angular spread is extremely narrow, and for head-on collisions $\ell_\perp = 0$, $q_\perp \approx \gamma_p \theta_p(\cos\psi, \sin\psi)$ where θ_p and ψ are the polar and azimuthal angles of the positron, and γ_p is the positron energy factor.

The functions I, F, and S are defined as

$$I = \int d\phi \left(1 - \frac{\ell \cdot \pi_p}{\ell \cdot p}\right) e^{i\Phi(\phi)},$$

$$F^\mu = \frac{1}{m} \int d\phi\, a^\mu(\phi) e^{i\Phi(\phi)},$$

$$S = \frac{1}{m^2} \int d\phi\, a(\phi) \cdot a(\phi) e^{i\Phi(\phi)},$$

with the exponent

$$\Phi(\phi) = \int_{\phi_i}^{\phi} d\phi' \frac{\ell \cdot \pi_p(\phi')}{m^2 \eta_\ell (1-s)}, \tag{2}$$

where π_p is the instantaneous momentum of the positron in the field

$$\pi_p = p - a + \frac{p \cdot a}{k \cdot p} k - \frac{a^2}{2k \cdot p} k. \tag{3}$$

The completed derivation of the NBW pair production probability could start from an S-matrix element with Volkov wave functions [45] and has been well documented in the literature (see, for example, [46] for an introduction and [12] for an analogous presentation for NLC). Because of the charge symmetry, the spectrum (1) can also be applied to the produced electron by just changing the corresponding definitions for the electron. After doing the transverse integral over $q_\perp$, the spectrum (1) shows the symmetry $P(s) = P(1 - s)$.

Quasimonoenergetic positron beams from chirped laser pulses

We now choose, as an example, the vector potential a^μ with circular polarization:

$$a^\mu(\phi) = m\xi[0, \cos\Psi(\phi), \sin\Psi(\phi), 0] f(\phi), \tag{4}$$

in which ξ and $f(\phi)$ are the normalized pulse amplitude and envelope, and $\Psi'(\phi) = \omega(\phi)/\omega_0$ is the chirped frequency of the pulse. Here and below, the prime ($'$) stands for the derivative of ϕ. For simple expression, we set the initial phase $\phi_i = 0$. At the initial phase, $f(\phi_i) = 0$ and $\omega(\phi_i) = \omega_0$.

We request (i) that the pulse duration is sufficiently long and the variation of the pulse local amplitude is much slower than the laser frequency, and (ii) that the variation of the local frequency $\omega(\phi)$ is on the same timescale as the pulse local amplitude (this will be clear later): $\omega'(\phi)$, $f'(\phi) \ll 1$. Under these conditions, we can then apply the *slowly varying* approximation that terms of order $f'(\phi)$ [$\omega'(\phi)$] can be neglected [47].

The exponent (2) can be expressed approximately as

$$\Phi(\phi) \approx \kappa(\phi)\phi - \zeta(\phi) \sin[\Psi(\phi) - \psi], \tag{5}$$

where we ignore all the terms proportional to $\omega'(\phi)$, $f'(\phi)$: $\int_{\phi_i}^{\phi} d\tilde{\phi}[\cos\Psi(\tilde{\phi}), \sin\Psi(\tilde{\phi})] f(\tilde{\phi}) \approx \omega_0[\sin\Psi(\phi), -\cos\Psi(\phi)] f(\phi)/\omega(\phi)$, and

$$\kappa = \frac{\ell \cdot p}{m^2 \eta_\ell (1-s)} + \frac{\xi^2}{2\eta_\ell (1-s)s} \frac{1}{\phi} \int_0^\phi d\tilde{\phi}\, f^2(\tilde{\phi}),$$

$$\zeta = \frac{\xi f(\phi)}{\eta_\ell (1-s)s} \frac{\omega_0}{\omega(\phi)} |q_\perp|.$$

With the Jacobi-Anger expansion:

$$e^{-i\zeta \sin(\Psi - \psi)} = \sum_{n=-\infty}^{+\infty} J_n(\zeta) e^{in\psi} e^{-in\Psi}, \tag{6}$$

where $J_n(\zeta)$ is the Bessel function of the first kind, the functions S can be expanded approximately as a series of harmonics:

$$S \approx -\xi^2 \sum_{n=-\infty}^{+\infty} e^{in\psi} \int d\phi\, f^2(\phi) J_n(\zeta) e^{i\Omega(\phi)}, \tag{7}$$

where $\Omega(\phi) = \kappa(\phi)\phi - n\Psi(\phi)$, the harmonic order n counts the net number of the laser photons absorbed from the background field. The dependence of the argument ζ on the pulse envelope $f(\phi)$ indicates that the contribution of each harmonic varies during the course of the pulse and the high-order harmonics contribute only at the pulse center where $f(\phi) \to 1$. The functions I and F can be calculated in the same way as (7) and obtained with exactly the same exponent term (and the different preexponents).

From (7), one can see that the main contribution to the functions I, F, and S, and therefore to the final spectrum (1), comes from the *stationary phase point* where

$$\frac{\partial}{\partial\phi}\Omega(\phi) = \frac{q_\perp^2 + m_*^2(\phi)/m^2}{2\eta_\ell(1-s)s} - n\frac{\omega(\phi)}{\omega_0} = 0, \tag{8}$$

where $m_*(\phi) = m[1+\xi^2 f^2(\phi)]^{1/2}$ denotes the effective mass of the produced positrons in the laser pulse [14,15].

Let us first consider the standard case with constant frequency: $\omega(\phi) = \omega_0$. The stationary condition (8) implies a chirp in the positron energy varying with the pulse envelope, $ds/d\phi \neq 0$: For the nth harmonic, the positron energy is in the spectral region $\tilde{s}_{n,-}(\phi) \leqslant s \leqslant \tilde{s}_{n,+}(\phi)$, where

$$\tilde{s}_{n,\pm}(\phi) = [1 \pm \sqrt{1 - 2m_*^2(\phi)/(n\eta_\ell m^2)}\,]/2, \tag{9}$$

shifting between the linear $[f(\phi) = 0]$ and nonlinear $[f(\phi) = 1]$ BW spectral lines. This shifting stems indeed from the variation of the positron's effective mass $m_*(\phi)$ during the course of laser pulse [20,22].

To exclude the energy chirp in the positron spectrum, one simple idea from (9) is to adapt the energy parameter η_ℓ by prescribing the laser frequency with a specific chirp, $\eta_\ell \sim \omega(\phi) \sim 1 + \xi^2 f^2(\phi)$, to compensate the variation of the particle effective mass in the laser pulse. As one can see, this frequency chirp is modulated by the field intensity and varies on the same timescale as the pulse envelope, satisfying the request before.

Based on the stationary condition (8), this frequency chirp can be prescribed by solving the differential equation

$$\frac{d\omega}{d\phi} = \frac{\omega_0}{2n\eta_\ell(1-s)s}\frac{d}{d\phi}[q_\perp^2 + 1 + \xi^2 f^2(\phi)], \tag{10}$$

with the initial conditions $f(\phi_i) = 0$ and $\omega(\phi_i) = \omega_0$, and acquired with its explicit expression

$$\omega(\phi) = \omega_0\big[1 + \xi^2 f^2(\phi)/(q_\perp^2 + 1)\big]. \tag{11}$$

From (11), one can see a remarkable fact that this chirp prescription is irrelevant to the harmonic order n, which indicates this spectral broadening can be removed from all the harmonic lines at the same time. One should also note that the complete counterbalance of the broadening can only happen at a particular outgoing angle $|q_\perp| \sim \gamma_p\theta_p$ specified by the chirp (11). For a realistic detector with nonzero angular acceptance $\Delta\theta > 0$, the spectral peaks of the probed positrons would shift slightly from the harmonic lines with a finite energy spread (see the results later in Fig. 4).

Similar discussions can also be applied to linearly polarized field backgrounds: $a^\mu(\phi) = m\xi[0, \cos\Psi(\phi), 0, 0]f(\phi)$, and the prescription of frequency chirp (11) is exactly the same, except that $\xi^2 \to \xi^2/2$.

III. NUMERICAL RESULT

In this section, we first present a numerical example of a head-on collision between a 13.1 GeV photon and a laser pulse with and without the frequency chirp, and then we consider the scenario in which the high-energy photon is replaced with a beam of γ photons obtained from the NLC process of a 16.5 GeV electron.

We are interested in the on-axis positrons collimated in the direction of the incoming photon $q_\perp \to 0$ for higher yield, and thus apply the frequency chirp:

$$\omega(\phi) = \omega_0[1 + \xi^2 f^2(\phi)]. \tag{12}$$

Inserting back into the stationary condition (8), one can then get the unchirped positron spectrum peaked at the angle $\theta_p = 0$ around the harmonic line

$$s_{n,\pm} = [1 \pm \sqrt{1 - 2/(n\eta_\ell)}]/2, \tag{13}$$

which can be understood as the linear BW harmonic in the collision between the incident photon ℓ^ν and a photon with momentum nk^ν. To produce a narrow-band positron beam at the cone angle $\theta_p \sim |q_\perp|/\gamma_p$, one can employ the frequency chirp (11).

To improve the interaction energy parameter η_l, we employ the laser pulse with the UV frequency $\omega_0 = 15.5$ eV and the envelope $f(\phi) = \sin^2(\phi/2N)$ where $0 < \phi < 2N\pi$ and $N = 16$. The (areal) energy of a plane laser pulse can be calculated as

$$E = -\frac{\omega_0}{4\pi\alpha\lambda\!\!\!^{-2}_e}\int d\phi\left(\frac{a'}{m}\right)^2, \tag{14}$$

in which $\lambda\!\!\!^{-}_e = 1/m = 386.16$ fm is the electron's reduced Compton wavelength. For circularly polarized laser pulses with the frequency chirp (12), one can obtain

$$E = \frac{\omega_0\xi^2}{4\alpha\lambda\!\!\!^{-2}_e}\left(\frac{3}{4} + \xi^2\frac{35}{32} + \xi^4\frac{231}{512}\right)N. \tag{15}$$

The first term within the brackets corresponds to the laser pulse with a constant frequency $\omega(\phi) = \omega_0$.

The choice of particle energy parameters is motivated by the upcoming high-energy experiments such as LUXE at DESY [38,39] and E320 at FACET-II [40,41]. The strong UV laser pulse can be obtained through the plasma harmonic generation driven by an ultrahigh-power optical laser pulse [42–44]. One of the potential methods to imprint the proposed frequency chirp into the laser spectrum is via the coherent superposition of two linearly and oppositely chirped laser pulses with suitable time delay [22].

A. NBW

Figure 1 depicts the narrowing of the positron angular spectra from the chirped laser pulse benchmarked with the results from constant-frequency pulses. As shown, the frequency chirp (12) can effectively compensate the broadening of each harmonic line: For the unchirped case in (b) and (c), where the laser, respectively, has the same energy or intensity as the chirped case in (a), harmonic lines are broadened with plenty of subsidiary peaks and overlap together to be a continuum spectral domain in the positron angular-energy distribution. However, for the chirped case in (a), the angular-energy distribution is comprised of a number of well-separated harmonic lines. Around each harmonic line, the distribution is narrowed to be a single peak at the small outgoing angle $\theta_p \to 0$ and is slightly broadened at larger scattering angles with some subpeaks, which comes from the interference between contributions from different stationary points. At the same time, the amplitude of the harmonic lines in the chirped case are significantly improved.

From Fig. 2(a), one can see that the chirped laser pulse can produce many more positrons than the unchirped case with the same intensity, and produce, approximately, the same number of positrons as the unchirped case with the same

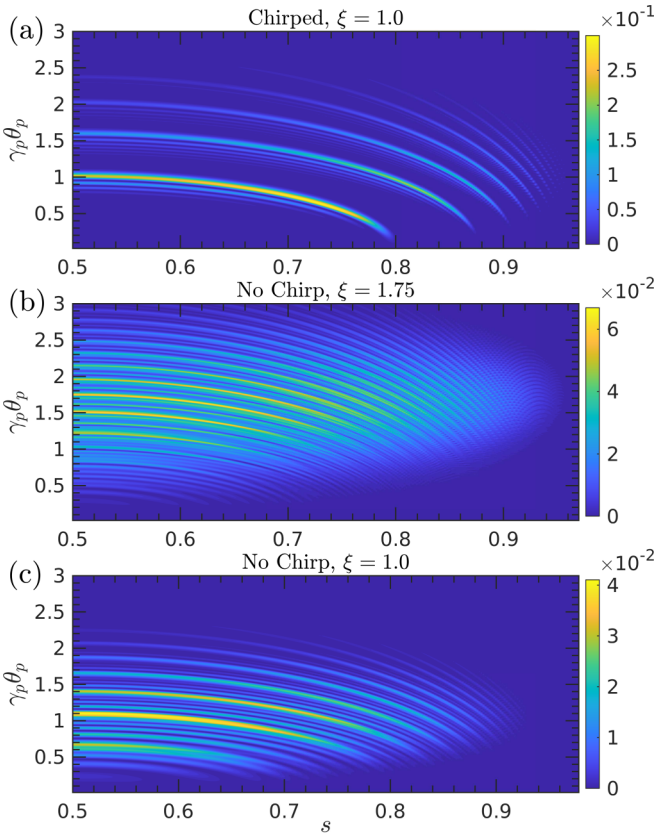

FIG. 1. Angular-energy distribution $d^2P/[ds\,d(\gamma_p\theta_p)]$ of the produced positrons via the NBW process from a high-energy photon (13.1 GeV) in a circularly polarized laser pulse with the proposed frequency chirp: (a) $\xi = 1$, and without the frequency chirp: (b) $\xi = 1.75$; (c) $\xi = 1$. The horizontal axis is restricted in the region $0.5 < s < 1$ because of the symmetry $P(s) = P(1-s)$. The chirped laser pulse ($\xi = 1$, $\omega(\phi) = \omega_0[1 + \xi^2 f^2(\phi)]$) has the same energy as the unchirped laser pulse ($\xi = 1.75$, $\omega(\phi) = \omega_0$).

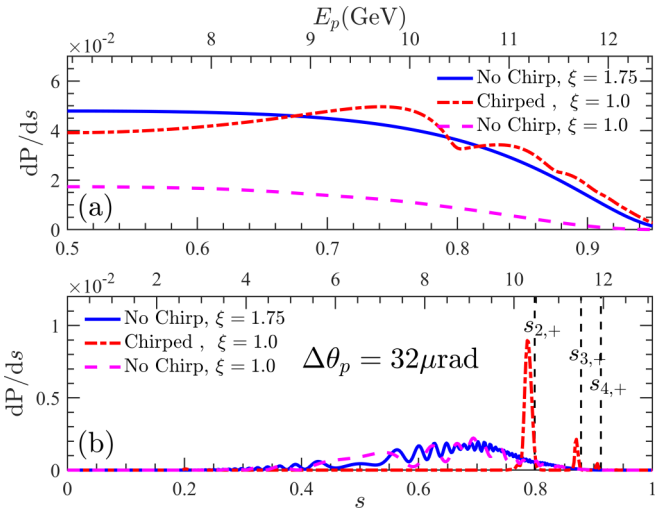

FIG. 2. Energy spectra dP/ds of the produced positrons shown in Fig. 1 within the whole angular spread, $\Delta\theta_p = \pi$ (a) and a narrow acceptance $\Delta\theta_p = 32$ μrad (b). For visibility, the spectral curve for the unchirped case is multiplied by a factor 10 for the $\xi = 1.0$ case and factor 20 for the $\xi = 1.75$ case in (b). The vertical dashed lines show the location of the first three harmonics in the chirped NBW process: $s_{2,+} = 0.80$, $s_{3,+} = 0.88$, and $s_{4,+} = 0.91$. On the top axis is shown the corresponding region of the positron energy $E_p \approx sE_\ell$. The other parameters are as in Fig. 1.

energy. The difference between the positron spectra appears around the harmonic lines $s_{n,\pm}$ (13), where the harmonic order n must be $\geqslant 2$ because of our parameter setup. This difference becomes significant in Fig. 2(b) where the angular-energy distribution is integrated within a narrow angular spread $\theta_p < \Delta\theta_p/2 = 16$ μrad: the positron spectrum from the chirped pulse background spikes around the harmonic lines $s_{n\geqslant 2,+}$ [see the vertical dashed lines in Fig. 2(b)], and has a much higher amplitude than that from the unchirped laser pulse which gives a much lower and broader spectrum in the on-axis direction. We label the location of the first three harmonics: $s_{2,+} = 0.80$, $s_{3,+} = 0.88$, and $s_{4,+} = 0.91$ in the chirped case. As one can see, the first spectral peak has a much higher amplitude and narrower energy spread $\Delta s/s \approx 1.7\%$ than other higher-order peaks, where Δs measures the full width at the half maximum of the peak. This collection of the positrons in a narrow high-energy region and particular direction can effectively improve the potential to observe this process in experiments.

The horizontal axis of the panels in Figs. 1 and 2(a) are restricted to the region $0.5 < s < 1$ because of the symmetry: $P(s) = P(1-s)$ [see Eq. (1) and the discussion above Sec. II].

However, the spectrum in Fig. 2(b), which is plotted for the whole spectral region $0 < s < 1$, shows an asymmetric distribution in the higher-energy region $s > 0.5$. This is because the lower-energy positrons distribute in a broader angular region: $\gamma_p \to 0$ leading to $\theta_p \to \pi/2$. Therefore, the lower-energy positrons could be simply excluded from the generated high-energy positron beam by an angular selection.

B. NLC + NBW

GeV γ rays generated by high-energy electron beams via the NLC process have been analyzed in detail in [4,48]. The spectrum of the emitted γ rays is presented in [12] in the same way as (1). With a similar stationary phase analysis, one can prove that a beam of quasimonoenergetic γ photons can be obtained in a well-chirped laser background [20]. Replacing the seed photon used in Fig. 1 with these acquired high-energy γ photons, a source of narrow-band positrons can be obtained. This two-step scenario can be regarded as a part of the trident process [49–51] in which only real photons contribute.

In Fig. 3, we plot the distributions of the emitted photons from a 16.5 GeV electron head-on colliding with the laser pulse parametrized as in Fig. 1(a). With the same technique as in the NBW case, the frequency chirp can effectively compensate the broadening of the photon spectrum, results in well-separated harmonic lines in the photon angular-energy distribution $d^2P_\gamma/d\theta_\ell dr$ in Fig. 3(a), especially for small angle scatterings $\theta_\ell \to 0$ [20,22], where $r = k\cdot\ell/k\cdot p_e$ is the fraction of the lightfront momentum taken by the scattered photon from the seed electron, p_e is the electron momentum, and θ_ℓ is the polar angle of the scattered photon.

With a narrow acceptance, $\Delta\theta_\ell = 16$ μrad collimated in the on-axis direction in Fig. 3(b), the collected photons

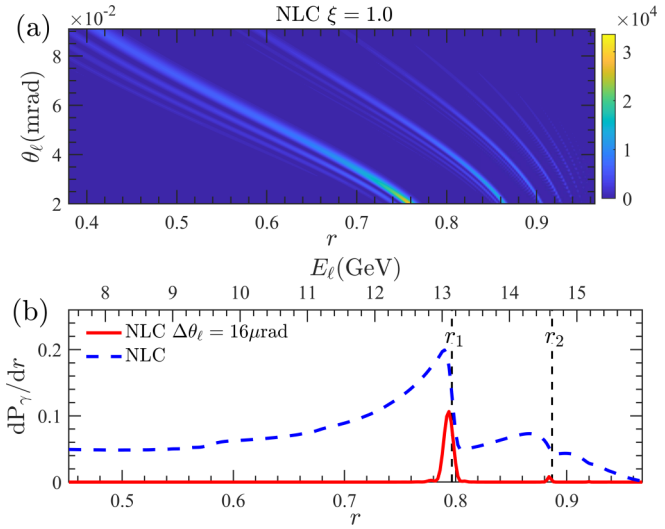

FIG. 3. (a) Angular-energy distribution $d^2P_\gamma/(dr\,d\theta_\ell)$ of the γ photons generated through the NLC process from a high-energy electron $E_e = 16.5$ GeV. (b) Energy distribution of the emitted γ photons within the whole angular spread, $\Delta\theta_\ell = \pi$ (blue dashed), and a narrow acceptance, $\Delta\theta_\ell = 16\,\mu$rad (red solid). On the top axis is shown the corresponding change in the photon energy $E_\ell \approx rE_e$ from 7.5 to 16 GeV. The vertical dashed lines show the location of the first two harmonics in the NLC process: $r_1 = 0.80$ and $r_2 = 0.89$ corresponding to the photon energy $E_\ell = 13.1$ GeV and 14.6 GeV. The laser parameters are the same as Fig. 1(b).

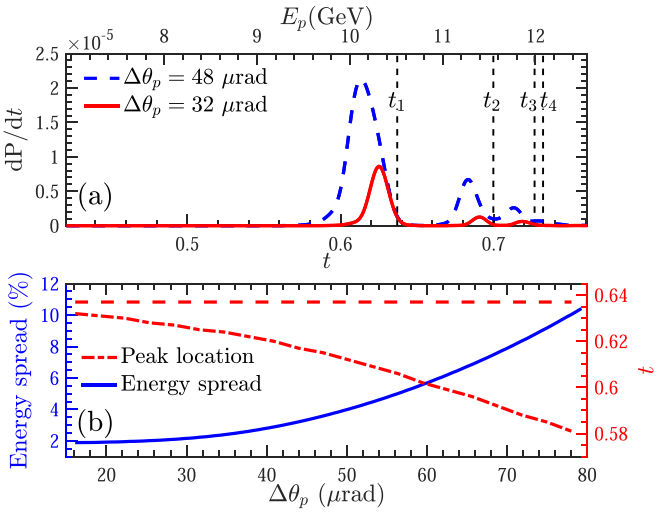

FIG. 4. (a) Energy distribution dP/dt of the positrons generated by the on-axis γ photons obtained through the NLC process of a high-energy electron $E_e = 16.5$ GeV. The energy region of the produced positron E_p is shown on the top axis. The vertical black dashed lines denote the location of each *combined* harmonic: $t_{1,2,3,4} = (0.637,\ 0.700,\ 0.726,\ 0.732)$ corresponding, respectively, to the energy $E_p = (10.5,\ 11.5,\ 12.0,\ 12.1)$ GeV. (b) Energy spread and peak location of the first harmonic peak with the change of the acceptance $\Delta\theta_p$. The horizontal dashed line denotes the theoretical location of the first *combined* harmonic: t_1. The energy spectrum of the γ photons used in the calculation is plotted as the red solid line in Fig. 3(b).

distribute tightly around the first harmonic line $r_1 = 0.80$, corresponding to the energy $E_\ell = 13.1$ GeV, with the energy spread $\Delta r/r \approx 1.3\%$, and subpeak around the second harmonic line $r_2 = 0.89$ at $E_\ell = 14.6$ GeV; see the vertical dashed lines in Fig. 3(b), where $r_v = 2v\eta_e/(2v\eta_e + 1)$, $\eta_e = k \cdot p_e/m^2$, $v \geqslant 1$ denotes the net number of laser photons absorbed in the NLC process. The other higher-order subpeaks are too small to view. With a broader angular selector $\Delta\theta_\ell = \pi$, the energy spread of the collected γ photons would be much larger, shown as the blue dashed line in Fig. 3(b).

Making use of the obtained γ-ray spectrum $\rho_\gamma(r) = dP_\gamma/dr$ in Fig. 3(b), we can calculate the total number of the generated positrons:

$$P = \frac{\alpha}{(2\pi\eta_e)^2}\int_0^1 dt \int_t^1 dr\,\rho_\gamma(r)h(r,t), \tag{16}$$

where $t = k \cdot p/k \cdot p_e$ denotes the fraction of the lightfront momentum transferring from the seed electron to the produced positron, and

$$h = \int d^2q_\perp \frac{|I|^2 + (SI^* + IS^* - 2F \cdot F^*)g(t,r)}{(r-t)rt}. \tag{17}$$

Here, we ignore the small angular spread of the collected γ photons to simplify the numerical calculations. The selection of small-angle photons can be done in experiments by adjusting the separation between the two laser pulses used in each process. This simplification would not affect the positron spectrum as the interaction parameter $\eta_\ell = k^0\ell^0(1 + \cos\theta_\ell)/m^2 \approx 2k^0\ell^0/m^2$ is almost unchanged. The induced error in the positron number would be much smaller than the total number of the collected positrons if the acceptance is much broader than the photon angular spread $\Delta\theta_p \gg \Delta\theta_\ell$.

In Fig. 4(a), we plot the yield of the positrons from the on-axis γ photons ($\Delta\theta_\ell = 16\ \mu$rad) obtained through the NLC process discussed in Fig. 3. With the acceptance $\Delta\theta_p = 32\ \mu$rad along the direction of the seed electron, most of the positrons are collected in a narrow energy region peaked at $t = 0.625$ with a narrow energy spread $\Delta t/t \approx 2.2\%$ and a much higher amplitude than other subpeaks in the higher-energy region. All of these peaks can be related to the *combined* harmonic lines $t_u = r_v s_{n,+}(r_v)$, where $s_{n,+}(r_v)$ is the value of the NBW harmonic line calculated with the NLC harmonic energy $\eta_\ell = \eta_e r_v$; see the vertical dashed lines in Fig. 4(a): The dominant peak is related to the first combined harmonic line $t_1 = r_1 s_{2,+} = 0.637$ corresponding to the energy $E_p \approx 10.5$ GeV. The one that appears around $t = 0.691$ corresponds to the second *combination* $t_2 = r_1 s_{3,+} \approx 0.700$ with the energy $E_p \approx 11.5$ GeV, and the one that appears around $t = 0.719$ may come from the sum of the combinations $t_3 = r_1 s_{4,+} = 0.726$ and $t_4 = r_2 s_{2,+} = 0.732$. The redshift of each peak location is because of the broad acceptance $\Delta\theta_p$ and can be reduced by narrowing the acceptance; see the red dot-dashed line in Fig. 4(b): the dominant peak moves asymptotically back to the location of the first *combined* harmonic line t_1 with a decreasing acceptance.

To improve the brilliance of the positron beam, one needs to increase the detector acceptance: with a larger acceptance $\Delta\theta_p = 48\ \mu$rad in Fig. 4(a), the amplitude of the spectral peak becomes much higher, and at the same time, its energy spread

is broadened to be 3.8%. As shown in Fig. 4(b), the energy spread of the probed positrons increases with the raising of the detector acceptance $\Delta\theta_p$. With a broad acceptance $\Delta\theta_p \approx 80$ μrad, one can acquire a positron beam with the energy spread around 10%, and with a relatively narrow acceptance $\Delta\theta_p < 56$ μrad, the energy spread of the positron beam can be simply controlled to be less than 5%.

IV. CONCLUSION

We investigated the nonlinear Breit-Wheeler process in a chirped laser background with intensity $\xi \sim 1$. Via the standard stationary-phase analysis, we elaborated the broadening of the produced positron spectrum stemming from its inhomogeneous effective mass during the course of the laser pulse, and proved that with a suitable frequency chirp, this broadening can be completely compensated in a specified direction. We present a proof-of-principle calculation in which a beam of quasimonoenergetic γ photons is obtained from a chirped laser pulse via the nonlinear Compton scattering process and then is used to produce electron-positron pairs in the second chirped laser pulse to provide a quasimonoenergetic source of positrons. The produced positrons are tightly gathered in a narrow energy region around the combine harmonic lines from the relevant processes. By adjusting the detector acceptance, the energy spread of the obtained positrons can be well controlled.

In our calculations, we ignore the energy spread of the seed electron beam, which would be crucial if it is in the same level of or much broader than the predicted positron energy spread. To obtain the predicted narrow-band positrons, high-quality electron beams with limited energy spread are needed [41]. We also ignore the radiation effect from the produced pairs before leaving the pulse, because the probability for this secondary radiation is much smaller than 1 in the intermediate intensity region $\xi \sim \mathcal{O}(1)$ [see the results in Fig. 3(b)] and thus can hardly affect the width of the positron spectrum. We employ the high-power laser pulse with the UV frequency which is critical in our discussion: the UV laser frequency guarantees the scattering of high-energy γ photons, and then significantly improves the yield of the electrons and positrons by opening the low-order harmonic channels for the following nonlinear Breit-Wheeler process.

ACKNOWLEDGMENTS

The author thanks Dr. A. Ilderton and Dr. B. King for useful discussion and careful reading of the manuscript. The author acknowledges support from the Young Talents Project at Ocean University of China.

[1] V. Ritus, J. Russ. Laser Res. **6**, 497 (1985).
[2] A. Di Piazza, C. Müller, K. Z. Hatsagortsyan, and C. H. Keitel, Rev. Mod. Phys. **84**, 1177 (2012).
[3] A. I. Nikishov and V. I. Ritus, Sov. Phys. JETP **19**, 529 (1964).
[4] B. King and S. Tang, Phys. Rev. A **102**, 022809 (2020).
[5] M. Boca and V. Florescu, Phys. Rev. A **80**, 053403 (2009).
[6] D. Seipt and B. Kämpfer, Phys. Rev. A **83**, 022101 (2011).
[7] F. Mackenroth and A. Di Piazza, Phys. Rev. A **83**, 032106 (2011).
[8] A. Ilderton and A. J. MacLeod, J. High Energy Phys. 04 (2020) 078.
[9] B. King, Phys. Rev. D **103**, 036018 (2021).
[10] K. Krajewska and J. Z. Kamiński, Phys. Rev. A **85**, 062102 (2012).
[11] T. N. Wistisen, Phys. Rev. D **90**, 125008 (2014).
[12] A. Ilderton, B. King, and S. Tang, Phys. Lett. B **804**, 135410 (2020).
[13] L. S. Brown and T. W. B. Kibble, Phys. Rep. **133**, A705 (1964).
[14] T. W. B. Kibble, Phys. Rev. **150**, 1060 (1966).
[15] H. R. Reiss, Phys. Rev. A **89**, 022116 (2014).
[16] E. Raicher and K. Z. Hatsagortsyan, Phys. Rev. Research **2**, 013240 (2020).
[17] F. V. Hartemann, A. L. Troha, N. C. Luhmann, Jr., and Z. Toffano, Phys. Rev. E **54**, 2956 (1996).
[18] T. Heinzl, D. Seipt, and B. Kämpfer, Phys. Rev. A **81**, 022125 (2010).
[19] F. Albert, S. Anderson, D. Gibson, R. Marsh, S. Wu, C. Siders, C. Barty, and F. Hartemann, Phys. Rev. ST Accel. Beams **14**, 050703 (2011).
[20] D. Seipt, S. G. Rykovanov, A. Surzhykov, and S. Fritzsche, Phys. Rev. A **91**, 033402 (2015).
[21] B. Terzić, K. Deitrick, A. S. Hofler, and G. A. Krafft, Phys. Rev. Lett. **112**, 074801 (2014).
[22] D. Seipt, V. Y. Kharin, and S. G. Rykovanov, Phys. Rev. Lett. **122**, 204802 (2019).
[23] G. Breit and J. A. Wheeler, Phys. Rep. **46**, 1087 (1934).
[24] H. R. Reiss, J. Math. Phys. **3**, 59 (1962).
[25] D. L. Burke, R. C. Field, G. Horton-Smith, J. E. Spencer, D. Walz, S. C. Berridge, W. M. Bugg, K. Shmakov, A. W. Weidemann, C. Bula *et al.*, Phys. Rev. Lett. **79**, 1626 (1997).
[26] C. Bamber, S. J. Boege, T. Koffas, T. Kotseroglou, A. C. Melissinos, D. D. Meyerhofer, D. A. Reis, W. Ragg, C. Bula, K. T. McDonald *et al.*, Phys. Rev. D **60**, 092004 (1999).
[27] N. B. Narozhnyĭ, Sov. Phys. JETP **28**, 371 (1969).
[28] M. J. A. Jansen, J. Z. Kamiński, K. Krajewska, and C. Müller, Phys. Rev. D **94**, 013010 (2016).
[29] T. N. Wistisen, Phys. Rev. D **101**, 076017 (2020).
[30] A. Titov, A. Otto, and B. Kämpfer, Eur. Phys. J. D **74**, 39 (2020).
[31] M. J. A. Jansen and C. Müller, Phys. Rev. A **88**, 052125 (2013).
[32] M. J. Jansen and C. Muller, Phys. Lett. B **766**, 71 (2017).
[33] A. I. Titov, H. Takabe, and B. Kämpfer, Phys. Rev. D **98**, 036022 (2018).
[34] A. Ilderton, Phys. Rev. D **101**, 016006 (2020).
[35] N. Cabibbo and R. Gatto, Phys. Rev. **124**, 1577 (1961).
[36] S. Myers and E. Picasso, Contemp. Phys. **31**, 387 (1990).
[37] S. Tang, A. Ilderton, and B. King, Phys. Rev. A **100**, 062119 (2019).
[38] A. Hartin, A. Ringwald, and N. Tapia, Phys. Rev. D **99**, 036008 (2019).

[39] H. Abramowicz, M. Altarelli, R. Aßmann, T. Behnke, Y. Benhammou, O. Borysov, M. Borysova, R. Brinkmann, F. Burkart, K. Büßer *et al.*, arXiv:1909.00860.
[40] C. Joshi, E. Adli, W. An, C. E. Clayton, S. Corde, S. Gessner, M. J. Hogan, M. Litos, W. Lu, K. A. Marsh *et al.*, Plasma Phys. Controlled Fusion **60**, 034001 (2018).
[41] S. Meuren, Probing strong-field QED at FACET-II (SLAC E-320). Talk presented at FACET-II Science Workshop 2019, https://conf.slac.stanford.edu/facet-2-2019/sites/facet-2-2019.conf.slac.stanford.edu/les/basic-page-docs/sfqed_2019.pdf.
[42] C. Rödel, D. an der Brügge, J. Bierbach, M. Yeung, T. Hahn, B. Dromey, S. Herzer, S. Fuchs, A. G. Pour, E. Eckner *et al.*, Phys. Rev. Lett. **109**, 125002 (2012).
[43] S. Tang, N. Kumar, and C. H. Keitel, Phys. Rev. E **95**, 051201(R) (2017).
[44] S. Tang and N. Kumar, Plasma Phys. Controlled Fusion **61**, 025013 (2019).
[45] D. M. Volkov, Z. Phys. **94**, 250 (1935).
[46] B. King, Phys. Rev. A **101**, 042508 (2020).
[47] T. Heinzl, B. King, and A. J. MacLeod, Phys. Rev. A **102**, 063110 (2020).
[48] S. Tang, B. King, and H. Hu, Phys. Lett. B **809**, 135701 (2020).
[49] V. Dinu and G. Torgrimsson, Phys. Rev. D **101**, 056017 (2020).
[50] V. Dinu and G. Torgrimsson, Phys. Rev. D **102**, 016018 (2020).
[51] G. Torgrimsson, New J. Phys. **23**, 065001 (2021).